Biochimica et Biophysica Acta, 645 (1981) 193–210
Elsevier/North-Holland Biomedical Press

BBA 79280

A STATISTICAL MECHANICAL TREATMENT OF FATTY ACYL CHAIN ORDER IN PHOSPHOLIPID BILAYERS AND CORRELATION WITH EXPERIMENTAL DATA

B. DIPALMITOYL-3-*sn*-PHOSPHATIDYLCHOLINE

JEAN-PAUL MERALDI [a] and JÜRGEN SCHLITTER [b]

[a] *Department of Biophysical Chemistry, Biocenter of the University of Basel, Klingelbergstrasse 70, CH-4056 Basel (Switzerland) and* [b] *Institute of Biophysics, University of Bochum ND/04, D-4630 Bochum (F.R.G.)*

(Received October 6th, 1980)
(Revised manuscript received January 15th, 1981)

Key words: Phospholipid bilayer; Statistical mechanics; Phase transition; ^{2}H-NMR order profile; Conformational probability; Spatial chain characteristics

In order to help bridge the conceptual gap between experimental data on chains of phospholipid molecules and their microscopic organization, a theoretical model has been proposed in a preceding paper. The intentions associated with the new theory were to describe a model able to reproduce accurately the experimental data. This capability is essential to monitor some of the mechanisms behind the physical data. The results presented here show first that, provided a suitable fitting of the phenomenological parameters entailed in the model, the theory indeed gives good agreement with experimental data (^{2}H-NMR, neutron scattering, calorimetry) obtained for a dipalmitoyl-3-*sn*-phosphatidylcholine bilayer. This property of the model is then specifically used to describe the nature of the perturbing effects of local anaesthetics and cholesterol on the organization of the acyl chains and to correlate these effects with the experimental data. Finally the theoretical model is used to supplement experimental data by describing the acyl chain organization in terms of the most probable spectrum of chain conformations. Predictions are made about the one-, two- and three-dimensional mean spatial characteristics of the acyl chains.

Introduction

As the phospholipid bilayer is recognized as an important component of biological membranes, it has been studied extensively by various physical techniques. A comprehensive picture of the thermotropic and lyotropic properties of these systems as well as their overall organization has resulted from such investigations [1]. Experimental data, however, although they are already highly informative, acquire a still deeper meaning at the molecular level if they can be reproduced and analyzed by means of a theoretical model. Moreover such a model can well supplement the experimental approach by giving access to physical quantities beyond the scope of the experiment.

The theoretical derivation of a model and its necessary parameters has been described in the preceding article [2]. For such a complex system as a phospholipid bilayer the theoretical problem can only be solved by the introduction of approximations. The very specific goals of a theory, however, narrow the choice of the approximations and determine the type of the model [2]. One of the aims of this paper is to investigate how thermodynamic averages over all possible chain configurations of the bilayer system might yield the orientational order data obtained from deuterium magnetic resonance (^{2}H-NMR) [3]. One related goal is to examine how the experimental data would be modified specifically when the distribution of the possible configurations is perturbed. To answer this type of question first it is necessary to consider a

physical situation and to reproduce exactly the experimental data. However such a model can only be solved by resorting to approximations. This condition leads to inclusion in the theory several phenomenological parameters of which the numerical values are obtained by data-fitting. The model uses in the partition function all the possible chain configurations (*trans*, *gauche* rotational isomers [4]). The principal assumptions were that the anisotropy of interaction between the chains is modified to account for the attractive forces by the molecular field approximation and for the short-range repulsive forces by a hard-core potential. The influence of the interactions in the polar head-group region on the area of one chain is accounted for by an effective lateral pressure.

The model is applied to analyze the thermotropic behaviour and describe the acyl chain organization of a dipalmitoyl-3-*sn*-phosphatidylcholine (DPPC) bilayer. In the first section starting from p_c, the theoretical expression for the statistical weight of any chain conformation, as derived in the preceding paper, numerical calculation of various thermodynamical quantities is carried out. A brief discussion of some of the computational aspects of this problem is also given.

In the main section we test first the capability of the model to reproduce experimental results from ^{2}H-NMR. Because of the good correlation it is then possible to compare changes in the ^{2}H-NMR experimental data with specific changes in the distribution of the possible acyl chain conformations. Thus conclusions can be made about the effect on the membrane of, for instance, local anesthetics or cholesterol. Moreover a new dimension can be added to the interpretation of ^{2}H-NMR data.

The predictions of the model regarding the macroscopic changes of the van der Waals and intramolecular energy are then compared to those yielded by the evaluation of recent dilatometry and calometry measurements [5]. The theory is then used to estimate for each CH_2 group along the chain the probability of all possible configurational states. This very detailed information is shown to give a much deeper insight into the understanding of the NMR data which by itself is limited to the description of angular fluctuations.

In the last part of the paper the model is concerned with the spatial distribution of the acyl chains. The neutron scattering data, which yields one-dimensional spatial information [6,7], are first reproduced. To elaborate more on the mean volume occupancy of the acyl chains the model is used to predict their three-dimensional spatial characteristics. Thus in one sense, the one-dimensional diffraction data can be extended to two- and three-dimensional space.

Theory

(a) The model

Eqn. 1, which expresses the conformational one-particle distribution function or simply the statistical weight of any chain conformation, summarizes the main result of the preceding paper [2].

$$p_c = \frac{1}{Z}\exp\left\{-\left[(2R_0 - \beta B_0)\,\sigma(c)\langle\sigma(c)\rangle - (2R_2 + \beta B_2)\right.\right.$$

$$\times \sigma(c)\sum_{j=1}^{N_s} P_2(\cos\theta_j(c))\langle\sigma(c)\cdot\bar{P}_2\rangle + \beta E_{int}(c)$$

$$\left.\left. + \beta\Pi A(c)\right]\right\} \qquad (1)$$

where Z is a normalization constant such that $\Sigma_c\, p_c = 1$. Here R_0, R_2 and B_0, B_2 are parameters which can be fitted to the experimental data and occur respectively in the repulsive and the attractive energies of interaction. N_s is the number of CH_2 segments and $\beta = 1/k_B T$. $\sigma(c)$ is a factor which accounts for the anisotropy of the energies of interaction on the overall shape of a chain conformation c. The arithmetic mean is defined by $P_2(\cos\theta(c)) = \frac{1}{N_s}\Sigma_{j=1}^{N_s}(3\cos^2\theta_j(c) - 1)/2$, where $\theta_j(c)$ is the angle between the normal to the bilayer and the normal to the plane spanned by the C-H bonds for the j^{th} carbon. This term describes the dependence of the anisotropy of the energies of interaction upon the mean orientation associated with a chain conformation. The bracketed variables signifying thermodynamic averages, $\langle\sigma(c)\rangle$ and $\langle\sigma(c)\bar{P}_2\rangle$, are the order parameters of the mean field formalism. The volume energy term $\pi A(c)$, where π is an effective lateral pressure and $A(c)$ the effective lateral chain area, accounts for the forces responsible for the interactions between headgroups and headgroup and water in the bilayer structure. The effective cross-sectional area $A(c)$ is equated to $A_0 L_0/$

$L(c)$ [8] where A_0 and L_0 are respectively the area and the length of the all-*trans* conformation. $L(c)$ is the effective length of the conformation (c), i.e. the projected length on the bilayer normal. The intramolecular energy $E_{int}(c)$ is evaluated by the rotational isomeric model [4]. Each carbon-carbon bond can take up either a *trans* (t) or a *gauche* conformation (g^+, g^-). The internal energy for a given conformation (c) is:

$$E_{int}(c) = E_1(c) + \sum_{j=2}^{N_s} E_{x_i, x_{i-1}}(c) \qquad (2)$$

$E_1(c)$ is the internal energy of the first segment and will be more fully discussed under part b) of this section. Here $x = t$, g^+ or g^-, $E_{x,t}(c) = 0$ and $E_{t,g^\pm}(c) = E_{g^\pm,g^\pm}(c) = 500$ cal/mol [4]. The sequence g^+, g^- and g^-, g^+ are excluded for steric reasons. Since in this study some of the results shall be compared to those given by the Marčelja [8] model, in this case the one particle distribution function is:

$$p_c = \frac{1}{Z} \exp\left\{ -\left[-\beta V_0 \frac{N_{tr}}{N_s}(c) \sum_{j=1}^{N_s} P_2(\cos\theta_j(c)) \right.\right.$$

$$\left.\left. \times \left\langle \frac{N_{tr}}{N_s} \bar{P}_2 \right\rangle + \beta E_{int}(c) + \beta \Pi A(c) \right] \right\} \qquad (3)$$

Most of the terms of Eqn. 3 have already been defined in describing Eqn. 1. V_0 is a coupling constant which will be used as parameter in fitting the theoretical model to the experimental data. In order to make effective the comparison between Eqn. 1 and 3 we set in Eqn. 1 $\sigma(c) = N_{tr}/N_s$, where N_{tr} is the number of segments in the *trans* configuration.

(b) The geometry

In all the computations presented in this paper the motion with respect to the axis of motional averaging defined as the normal to the bilayer is considered to arise solely from chain isomerisation. Rigid body motion, which has been suggested to occur in bilayers [9] has not been included, since it seems that this type of motion is not compatible with some observed data (Meraldi, J.-P., unpublished results). However, for the present calculation this deliberate choice will be considered as an assumption.

According to the formalism of the model (see Ref. 2), the hydrocarbon chain is identified with a sequence of vectors $\bar{v}_i$ linking the middle points of two adjacent C-C bonds as depicted in Fig. 1A. The conformational state of a chain is therefore completely described by the rotameric state (t, g) of each CH_2 monomer and the polar angle θ with respect to the bilayer normal of each $\bar{v}$ vector, as illustrated by a few examples in Fig. 1B. The practical evaluation of the conformations is achieved by attaching a laboratory frame of reference to the bilayer normal (Z axis parallel to the bilayer normal) and a molecular axis to each CH_2 monomer as defined in Fig. 1C. With these definitions a vector $\bar{v}_j = b \cdot \bar{u}_j$, where $\bar{u}_j$ is a unit vector and b the length of the vector, is obtained in the laboratory system from the following equation:

$$\bar{u}_j^L = T_j T_{j-1} \ldots T_1 \bar{u}^L \qquad (4)$$

where $\bar{u}^L$ is a unit vector with coordinate (0, 0, 1) and the T's are orthogonal transformation matrices. In the case of T_j the $j - 1^{th}$ system is transformed into the j^{th}. $\bar{v}_j^L$ is equal to $b \cdot \bar{u}_j^L$ whereas its director cosine with respect to the bilayer normal is $(\bar{u}_j^L)_Z =$

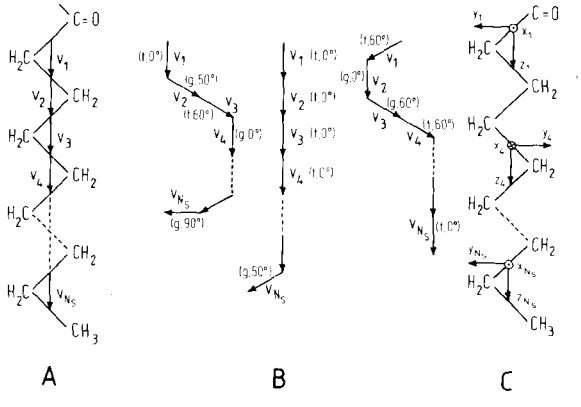

Fig. 1. Schematic representation of the chain conformations and the definition of the different coordinate systems attached to each molecules. (A) The CH_2 groups are replaced by $\bar{v}_j$ vectors connecting the midpoints of consecutive segments. (B) Examples are given of chain conformations in the segmental representation, where (x, θ) specifies the rotemeric state of the individual segments. x stands for *trans* (t) or *gauche* (g) and θ is the polar orientation of the segment and is shown in degrees, i.e., 0°, 60°, etc. (C) This defines the molecular axes attached to each CH_2 monomer, where x_j, y_j and z_j represent an orthogonal system.

$\cos\theta_j$. Taking the C-C bond angles as tetrahedral, the matices T_2 to T_j, which express each one of the three rotational states are of one of the following types:

$$T(t) = \begin{bmatrix} -1 & 0 & 0 \\ 0 & -1 & 0 \\ 0 & 0 & 1 \end{bmatrix}$$

$$T(g^+) = \tfrac{1}{2}\begin{bmatrix} 1 & \sqrt{2} & 1 \\ -\sqrt{2} & 0 & \sqrt{2} \\ 1 & -\sqrt{2} & 1 \end{bmatrix}$$

$$T(g^-) = \tfrac{1}{2}\begin{bmatrix} 1 & \sqrt{2} & -1 \\ \sqrt{2} & 0 & \sqrt{2} \\ -1 & -\sqrt{2} & 1 \end{bmatrix} \qquad (5)$$

T_1 is related to the possible orientations of the first chain vector. Experimentally, however, nothing is accurately known about the possible orientational states of the vector $\bar{v}_1$ and their contributions to the internal energy the term $E_1(c)$ given in Eqn. 2. The simplest way to overcome this difficulty is to assume orientational state of the same kind as for the other chain vectors, i.e., states which may be described by the matrices (Eqn. 5) or combinations of these matrices. We choose therefore three orientations, introduced by Schindler and Seelig [10], which are best defined by introducing two virtual vectors preceding the first one as following: *tt/t*, *tt/g* and *tg/t*. The energies which effectively weight each state are assumed to be those which give the best fit of the deuterium quadrupole coupling of the first methylene group.

The length $L(c)$, needed for the expression $A(c) = A_0L_0/L(c)$, is given by

$$L(c) = b\sum_{j=1}^{N_s}\cos\theta_j(c) \qquad (6)$$

Since the chains have to exist in a bilayer structure, $L(c)$ can never become negative. This is the only restriction on chain isomerization. For the numerical computation $b = 1.27$ Å and $A_0 = 20$ Å [11]. Chain one and chain two are considered as equivalent and formally the phospholipid molecules are treated as one chain.

(c) Some aspects of the computer program

The first step in the numerical analysis is to evaluate the molecular fields, the so-called order parameters of the mean field formalism $\langle N_{tr}/N_s\rangle$ and $\langle N_{tr}\cdot\bar{P}_2/N_s\rangle$ in Eqn. 1. This is achieved by solving iteratively the system of self-consistent equations.

$$\left\langle\frac{N_{tr}}{N_s}\right\rangle = \sum_c p_c N_{tr}(c)/N_s$$

$$\langle N_{tr}\cdot\bar{P}_2/N_s\rangle = \sum_c p_c N_{tr}(c)\,\overline{P_2(\cos\theta(c))}/N_s \qquad (7)$$

In the neighbourhood of the order-disorder transition, the system of Eqn. 7 displays two stable solutions corresponding to the gel and the liquid crystalline states [2]. The final numerical evaluation of the molecular fields occurs when the free enthalpies of both states are equal.

For each step of iteration the solution of the Eqn. 7 involves an evaluation of all the relevant conformations and their respective statistical weights. Since the generation of the conformations is the most time-consuming part of the computation, it is important to do this only once. However during the iterative solution, it is not possible to store each individual conformation. To solve this problem the follwoing procedure has been used. The greatest possible part, which remains unchanged during iteration, is extracted by rewritting the partition function as a double integral over the ranges of the molecular fields. The integrals are then converted into sums in the usual way.

$$Z = \sum_c \exp\left\{-\left[(2R_0 - \beta B_0)\frac{N_{tr}}{N_s}(c)\left\langle\frac{N_{tr}}{N_s}\right\rangle - (2R_2 + \beta B_2)\frac{N_{tr}}{N_s}(c)\cdot\sum_{j=1}^{N_s}P_2(\cos\theta_j(c)) \times\left\langle\frac{N_{tr}}{N_s}\cdot\bar{P}_2\right\rangle + \beta E_{int}(c) + \beta\Pi A(c)\right]\right\}$$

$$= \int_{(N_{tr}/N_s)_{min}}^{(N_{tr}/N_s)_{max}} dx \int_{(N_{tr}\cdot\bar{P}_2)_{min}}^{(N_{tr}\cdot\bar{P}_2)_{max}} dy \times \underbrace{\left[\sum_c e^{-\beta(E_{int}(c)+\Pi A(c))}\,\delta\left(x - \frac{N_{tr}}{N_s}(c)\right)\right]}_{\rho(x,y)}$$

$$\times \delta(y - N_{tr}(c)\,\overline{P_2(\cos\theta(c))}\Big]$$

$$\times \exp\left\{-\left[(2R_0 - \beta B_0)\left\langle\frac{N_{tr}}{N_s}\right\rangle x\right.\right.$$

$$\left.\left. - (2R_2 + \beta B_2)\left\langle\frac{N_{tr}}{N_s}\cdot \bar{P}_2\right\rangle y\right]\right\}$$

$$\cong \sum_{i=1}^{N_x}\sum_{j=1}^{N_y} \rho_{ij} \exp\left\{-\left[(2R_0 - \beta B_0)\left\langle\frac{N_{tr}}{N_s}\right\rangle x_i\right.\right.$$

$$\left.\left. - (2R_2 + \beta B_2)\left\langle\frac{N_{tr}}{N_s}\cdot \bar{P}_2\right\rangle y_i\right]\right\} \qquad (8)$$

The necessary information about the conformations is contained in the weight density matrix ρ_{ij} which has to be calculated only once. The accuracy of the sum approximation can be tested by varying the number of intervals, N_x and N_y. Typically values of N_x and N_y of 30 were used and by taking advantage of all the symmetries in generating the conformations, the programme runs in a UNIVAC 1100/81 in roughly 1 min and uses less than 40K of memory.

Results and Discussion

(a) The ^{2}H-NMR order profile

In an external magnetic field, H_0, parallel to the bilayer normal (the axis of monotional averaging), the quadrupole splitting of a deuteron attached to the i^{th} carbon atom, i, is

$$\Delta\nu_i = \frac{3}{2}\frac{e^2qQ}{h} S_{C^2H_i} \qquad (9)$$

where

$$S_{C^2H_i} = \left\langle\frac{3\cos^2\beta_i - 1}{2}\right\rangle.$$

Here e^2qQ/h is the static quadrupole coupling constant and β the angle between the bilayer normal and the C-^{2}H bond [3]. The brackets means that all of the orientations of the C-^{2}H bond with respect to the axis of symmetry have been averaged. The set of $S_{C^2H_i}$ values obtained when the deuterated carbon is moved through the acyl chain yields the so-called order profile. It is characteristic of the segmental order within any defined bilayer [3,12,13].

The theoretical model is first used to reproduce the experimental order profile determined for chain one of a bilayer consisting of dipalmitoyl-3-*sn*-phosphatidylcholine at the phase transition temperature, 314 K [14]. This is achieved by adjusting the parameters R_0, R_2, B_0, B_2 and $E_1(c)$ in Eqn. 1 for an optimal fit and by requiring in addition the equality of the free enthalpy in the gel and liquid crystalline phase. The result is shown in Fig. 2A (top curve) where the symbols correspond to the experimental data. This fit is, however, sufficient only to determine the numerical difference $(2R_0 - \beta B_0)$ and the sum $(2R_2 + \beta B_2)$. The entropy change ΔS at the phase transition and the temperature dependence of the order parameters can be used to obtain the individual constants. ΔS, as determined by calorimetry, is the sum of various entropy contributions, which experimentally, are not individually accessible. These are: the intra-chain melting entropy, the spatial disordering entropy and the entropy of the water molecules interacting with the head groups. The model, however, yields only the intra-chain melting entropy. In order to compare the experimental and the theoretical data, it is necessary to estimate the spatial dis-

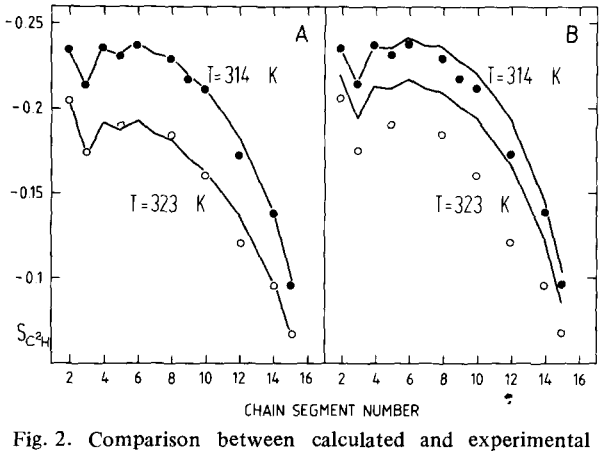

Fig. 2. Comparison between calculated and experimental S_{C^2H} order profiles. The results are shown at the phase transition remperature, T_c = 314 K and at T = 323 K Fig. 2A uses the method in reference [2] while Fig. 2B contains curves resulting from the Marčelja model. The experimental data are taken from Seelig and Seelig [14] and are shown by the points. The lines represent the theoretical results.

ordering entropy and the entropy contribution of the water molecules. If the bilayer is undergoing an endothermic phase transition, the membrane surface expands. More water molecules should become organized in the polar head group region, so the entropy contribution to ΔS should therefore be negative [15]. To estimate this negative entropy contribution we may combine the two following observations. According to Nagle and Wilkinson [5] a minimum of $N_s = 6$ chain segments is necessary to guarantee the existence of a sharp cooperative phase transition. According to Seelig [15] the overall entropy change is linearly related to the chain length. The negative entropy may be estimated by extrapolating in the curve of ΔS vs. N_s to $N_s = 5$. The result is ΔS (H_2O) = −4.0 (e.u./mol). The extrapolation is subject to error since the experimental set of data is insufficient to justify linear relationship.

The spatial disordering entropy has been estimated to be of the order of 1.0 e.u./mol [16], this yield finally for DPPC, an intra-chain melting entropy per CH_2 segment of 0.96 e.u./mol CH_2. Use of the Clausius-Clapeyron equation with the numerical values given in the work of Nagle and Wilkinson [5] yields $\Delta S = 0.905$ e.u./mol CH_2. The R_0, R_2, B_0, B_2 constants are therefore recalculated to give the best fit of the temperature dependence of the order parameters and simultaneously this value of the entropy change at the phase transition. However, it must be noted that beyond an entropy range of $0.87 \leqslant \Delta S(CH_2) \leqslant 1.04$, a reasonable fit of the temperature dependence is no longer obtainable independent of the values of the R_0, R_2, B_0 and B_2. Moreover, in the above entropy range, the best fit of the temperature dependence for R_0, R_2, B_0 and B_2 in each case gives about the same set of values.

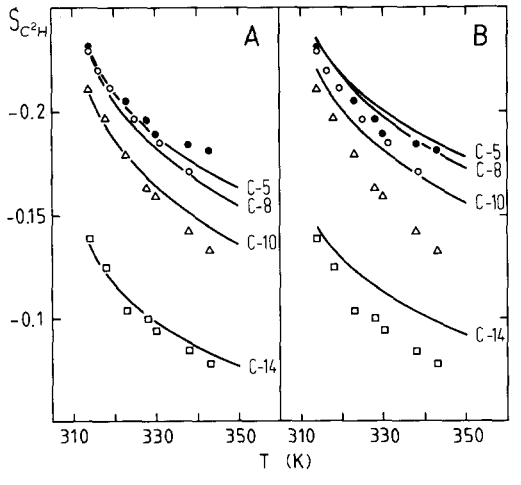

Fig. 3. Comparison between calculated and experimental S_{C^2H} order parameter of CH_2 segments 5, 8, 10 and 14 as a function of temperature. The lines shown in Fig. 3A are the theoretical results from this model, while Fig. 3B contains the results from the Marčelja model. The experimental data are taken from Seelig and Seelig [14] and are indicated by the points.

To give a striking example of the ability of the model to reproduce the temperature dependence of the order parameters, they have been computed in two different situations. In Fig. 2A (bottom curve) the entire order profile is simulated at $T = 323$ K ($T_c = 314$ K) and the result is again compared to the experimental data (symbols). In Fig. 3A four order parameters of representative C^2H_2 segments, namely, 5, 8, 10 and 14, are simulated over a large range of temperature (314 K to 350 K) and are compared to the experimental points (symbols). The numerical values of all the input parameters needed to perform the simulations are listed in Table I.

As already pointed out in the preceding paper, the numerical values of R_0 and R_2 as shown in Table I cannot be related to physical properties. Instead these parameters express the mean values of some geometrical properties of the chains not precisely expressed by the order parameters of the molecular field theory. However they are essential for reproducing the strength of the intermolecular interactions. B_0 and

TABLE I

INPUT PARAMETERS OF THE ONE-CHAIN DISTRIBUTION FUNCTION

R_0/CH_2	0.4229 (mol CH_2)$^{-1}$
R_2	0.1602 (mol CH_2)$^{-1}$
B_0/CH_2	632.7 (cal/mol CH_2)
B_2	352.0 (cal/mol CH_2/
A_0	20.0 Å^2
b	1.27 Å
Π	14.7 dyn/cm
E_g	500 cal/mol
E_1 (tt/t)	0.0 cal/mol
E_1 (tt/g)	−200.0 cal/mol
E_1 (tg/t)	−360.0 cal/mol

B_2 are coupling constants of the van der Waals forces. However, the anisotropy of the attractive interaction arises chiefly from the anisotropy of the hard-core repulsions and B_0 and B_2 are not pure coupling constants in the formalism of the model. Like R_0 and R_2 they express some mean geometrical properties of the chain molecules. Some physical bounds on these variables can be determined. The sum of B_0 and B_2 must not exceed 1.184 kcal/mol, the sublimation energy of a CH_2 monomer [17]. The best fit values given in Table I fulfill this requirement.

Even though it is not possible to relate the numerical values of R_0, R_2, B_0 and B_2 with physical constants, their role with regard to order in both phases and the strength of the first-order phase transition can be described. An increase in the value of R_2 or B_2 results in a greater increase in the order in the gel phase than in the fluid phase and leads to a stronger first order phase transition. Conversely, an increase of R_0 reduces the order in both phases, but by a greater amount in the gel phase. In that case there is a weaker first-order phase transition. Finally, the order will increase more in the fluid phase than in the gel phase when B_0 is set to a higher value. Therefore when the values of R_2, B_2 and B_0 are increased independently the phase transition will be shifted to higher temperatures. T_c is shifted to lower values when R_0 is increased. All of these parameters influence the shape of the simulated order profile, it being noted, however, that their contribution to the statistical weight of each chain conformation is different. However, these effects are not very large. More important is the possibility of obtaining a suitable value of the lateral pressure, which can be done by altering the relative values of the simulation parameters, and fulfill the conditions for a phase transition. As it will be shown subsequently the laterall pressure has an important effect on the shape of the order profile. the best fit of the order profile is obtained with an effective lateral pressure of $\pi = 14.7$ dyn/cm.

According to Hui et al. [18] and Nagle [19], π should be equal to 50 dyn/cm. This value is based on the idea that at this pressure, a monolayer exhibits a bilayer-like packing. In contrast, Albrecht et al. [20] proposed that a monoleyer and a bilayer are in an equivalent state when the changes in area and entropy at the phase transition are equal. Thus they found a π value for a DPPC bilayer of 12.5 dynes/cm. Finally Blume [21] claimed that both systems are equivalent when the absolute area and the area change are the same, finding thus for π (DPPC) a value of 30 dyn/cm. In the simulation studies, it would be easiest to assume that the definition of Albrecht et al. [20] is the most appropriate. However rather than adopting any of the aforementioned values, we are proposing that both systems are equivalent when the reduced variables are equal [22]. This definition implicitly assumes the existence of a critical point for a bilayer [14,23,24]. The critical point for our model is found to occur at 328 K and 31 dyn/cm. For a monolayer of DPPC the corresponding experimental parameters are respectively 316 K and 45 dyn/cm [20]. Therefore, according to the reduced variables procedure, the phase transition of a DPPC bilayer at 314 K and 14.7 dyn/cm should correspond to a phase transition of a DPPC monolayer at 302.5 K and 21.3 dyn/cm. The lateral pressure-area diagram of a DPPC monolayer published by Albrecht et al. [20] shows that the prediction of the model is verified to within less than one percent. Hence the value of 14.7 dyn/cm is at least consistent within the frame of the theoretical model.

Unlike the parameters R_0, R_2, B_0, B_2, π is a very important parameter in the simulation of the overall shape of the order profile. This is illustrated in Fig. 4 where the order profile of DPPC has been calculated under three different pressures. The most noticeable change is in the width of the plateau region. An increase in the lateral pressure results in a broadening of the plateau, whereas the plateau tends to disappear as the pressure is decreased. Parenthetically, Fig. 4 also illustrates how the pressure shifts the phase transition temperature as each theoretical profile has been obtained under the conditions of a phase transition. Fig. 4 reproduces qualitatively the experimental results of Mely et al. [25] obtained on a potassium laurate/water system where the water content of the lamellar phase was varied. Since the area per polar head is changing with changes in the water concentration, the observed effects on the plateau have to be attributed to changes in the magnitude of the lateral pressure.

The bottom profile of Fig. 4 provides an explanation for the shortening of the order profile plateau observed when molecules of benzyl alcohol, a local anaesthetic, are added to a bilayer [26]. It may be

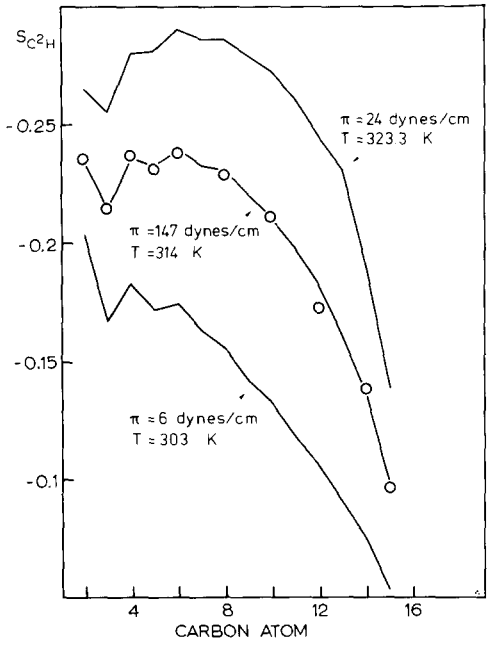

Fig. 4. Effect of the magnitude of the lateral pressure π on the order parameter profile. The order parameter profile has been simulated with three different values of the lateral pressure and the temperature corresponding to the condition of a phase transition. The open circles are the experimental data [14]. Of particular interest are the modulation of the length of the order profile plateau and of the phase transition temperature by the magnitude of the lateral pressure. Fig. 4 reproduces qualitatively the effects observed on lamellar soap/water systems when the content of water is varied [25]. The bottom curve of Fig. 4 shows the qualitative correspondence to the changes observed in the order profile of DMPC when benzyl alcohol, a local anesthetic, is added to the bilayer [26].

deduced that the perturbating molecules are sitting at the interfacial region of the glycerol backbone acting as spacers between phospholipid molecules [27]. This results in a decrease of the effective lateral pressure and thereby a shortening of the plateau.

Another conformational parameter, which does not appear explicitly in Eqn. 1 but also influences the length of the plateau, is the degree of hairpin or loop bending of the hydrocarbon chains. In the preceding section discussing chain geometry, it was specified that, in order to deal with the most general case, no special restriction is given to chain isomerizations within the limits of the rotameric model. Since most of the published models [28,34] eliminate a priori the loop of a hydrocarbon chain as being unrealistic, the simulation presented in Fig. 2A (top curve) has been repeated with this restriction to test the effect on the theoretical results. The best fits of the order profiles at T_c for the restrictive condition (no loop allowed) are shown in Fig. 5 and differ notably if the whole chain or only the first eight CH_2 segments are included. The effect on the width of the plateau, especially in Fig. 5a, which represents the result for no allowed loop conformation, is dramatic. Again this observation may be linked to an actual situation in certain ^{2}H-NMR measurements. Indeed one of the most noticeable effect on the shape of the order profile in the presence of cholesterol, is a broadening of the plateau region [26]. Clearly the rigid choles-

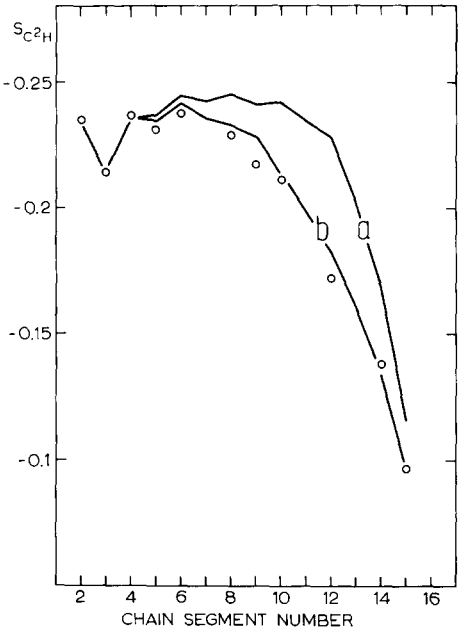

Fig. 5. The sensitivity of the theoretical profile to a priori conditions on the distribution of the possible chain conformations. Two examples of calculated order profiles are given and compared with the experimental data [14] indicated by the open circles. In one case (a), the segments have not been allowed to fold back whereas in (b) only the first light segments cannot fold back. Note in case (a) the dramatic influence on the length of the plateau of the order profile, an effect which is qualitatively observed when cholesterol is added to the bilayer [26]. The results illustrate how the rigid cholesterol molecule eliminates many possible acyl chain conformations.

terol molecule sterically prevents the acyl chains from folding back, thus reducing the extent of chain isomerisation. The same phenomena is likely to be the basis of a slightly larger plateau region for acyl chain one as compared to chain two for DPPC [14]. As the two hydrocarbon chains occupy different depths in the bilayer [35,36] chain two is more restricted in the ability to form loop conformations than chain one. The result is a lengthening of the plateau. Finally it is important to note that the plateau does not tend to disappear with a decreasing lateral pressure if the loop conformations are not allowed in the calculation.

In order to evaluate the statistical model proposed here with existing models some comparative calculations were carried out. For example, the Marčelja model given by Eqn. 3 [8] is compared in Figs. 2B and 3B with that of the present model and with the experimental ^{2}H-NMR data, again given by the discrete points. The comparison of the two models is interesting because they are of the same type but differ primarily in the nature of the anisotropic interactions between the acyl chains [2]. The differences in the results of the two models offer therefore a good opportunity to evaluate the suitability of different theoretical approaches. At the phase transition (top curve of Figs. 2A and 2B) both models give almost equally good simulations of the experimental order profile. In Fig. 2B at 314 K the simulated plateau is somewhat broader than that from the experimental results. This broadening in the Marčelja simulation arises from the need for a higher value of the lateral pressure π to ensure that the free enthalpies of both phases are equal at the phase transition. Comparison of the bottom curves of Fig. 2 as well as Fig. 3A with Fig. 3B illustrates even more striking differences between the theoretical models. In the present model, the anisotropy of the short-range intermolecular repulsions are introduced as the dominant factor governing intrinsic order among the chains, while the anisotropy of the attractive forces plays a somewhat secondary role [2]. In the Marčelja model only this last contribution is used. The short-range repulsions, which are described by a hard-core potential leading to Eqn. 1 result in a set of variables largely independent of temperature. Such an approach accounts for the improved thermal behaviour of this model over the Marčelja model. It should be clear, however, that with this result, we are not trying to justify a posteriori the use of more open parameters than in the Marčelja theory.

(b) Change of thermodynamic quantities for DPPC at the phase transition

The gel-to-liquid crystal transition involves different energetic contributions which are individually not directly obtainable. Using an elegant combination of calorimetry and dilatometry and a simple theoretical model, Nagle and Wilkinson [5] recently succeeded in calculating the change of the rotamer energy and of the van der Waals energy for the thermal transition. Since the present model yields another way of calculating these energies it is interesting to carry out a comparison between the two approaches. The results are given in Table II and they were obtained with the input parameters for the simulated order profiles as given in Table I. The agreement between the two van der Waals energies is excellent, whereas our figure for the rotamer energy is slightly smaller than that of Nagle and Wilkinson. It should be noted that the value of this energetic contribution given by Nagle and Wilkinson is an estimate rather than experimentally derived. The similarity in the results from the two models is very important since it demonstrates that once the parameters of Eqn. 1 have been adjusted on the basis of experimental data such as the ^{2}H-NMR results, the distribution function may then be used reliably to compute data not accessible experimentally.

Table II also contains the values of the order parameters of the molecular field formalism. They are mentioned here only to give a rough idea about the extent of discrete change in the conformational order at the phase transition. The mathematical formula leading to the entropies S(mixing) and S(packing) have been given in the preceding paper [2].

(c) Probability of individual segmental configurations

The S_{C^2H} order parameter is a measure of the extent of angular fluctuation with respect to the axis of monotional avaraging [37]. The angular fluctuation is due to rapid conformational isomerizations. In other words each chain segment has a probability of existing in several different configurations and the measured S_{C^2H} order parameter is the macroscopic averaged value of the order parameters corresponding

TABLE II

THERMODYNAMIC QUANTITIES FOR DPPC AT THE PHASE TRANSITION

Molecular fields			Intrachain melting entropies per phospholipid		Energies (kcal/mol)		
$\left\langle \frac{N_{tr}}{N_s} \right\rangle$	gel	0.926	ΔS (mixing)/R	13.69	ΔU (rot)	2.43 *	2.8 **
	fluid	0.723	ΔS (packing)/R	1.77	ΔU (vdW)	5.56 *	5.6 **
	gel	0.778	ΔS (total)/R	15.46			
$\left\langle \frac{N_{tr}}{N_s} \cdot \bar{P}_2 \right\rangle$							
	fluid	0.2813					

* This model.

** Nagle and Wilkinson [5].

to each of these different states. It is the purpose of this section to explain the values of the order parameters in terms of the probability of these segmental configurations, Sterically favorable sequences involving three and five segments in a row have been given the name of 'kink' and 'jog', respectively [38,39]. Both have been shown to occur with a rather low probability [10]. Nevertheless the kink structure is felt still to be important. Most of the conformational events in the acyl chains are thought to be related to the existence of kinks [29,32, 40,41]. Therefore the occurrence of these two defects will be discussed in this section too.

As indicated earlier, combinations of the T matrices (Eqn. 5) yield for the $\bar{v}$ vector a set of five possible polar orientations with respect to the bilayer normal, namely 0°, 60°, 90°, 120° and 180°. According to the type of the $T_j$matrix in Eqn. 4, the j^{th} segment is said to be either in a *trans* (t) or in a *gauche* (g) state. Hence each segment is doubly characterized and can exist in ten different configurations. The probability for each segment along the chain to exist in one or the other of these configurations is shown in Fig. 6. The first segment has been purposely omitted in Fig. 6. The main characteristic of the order profile, a plateau and decreasing order toward the end of the chain, are apparent from the different probability profiles. In addition, it is interesting to note that probabilities of the configurations involving polar orientations larger than 90° are not negligible. Such configurations correspond to a loop conformation of the acyl chain. This result confirms the previous finding showing the importance of these configurations on the shape of the order profile.

Fig. 6 contains also the probabilities of existence of a kink conformation as a function of the position along the chain. The low probability of this conformational defect is in close agreement with previous results [10]. A value of 0.51 kink per palmitic acyl chain and therefore roughly one kink per DPPC molecule at T_c has been determined. In agreement with previous estimated [10,42,43] and Raman data [44] the calculation predicts an average number of 20 bonds in the *trans* state and eight in the gauche configuration per DPPC molecule. Therefore the kink formation contributes only 25% to the rotamer energy. By considering in addition the jog conformation (0.17 jog per palmitic acyl chain) a total contribution of 33% from these two defects to the rotamer energy is obtained. If the disorder in the chains is evaluated by the average number of bonds which are not in the (t, 0°) configuration it is found that the kinks and the jogs taken together represent 27.5% of the observed disorder. Hence these two specific types of conformer cannot be the principal component of the observed disorder. Moreover, the kink form was shown to be in conflict with the dilatometry and calorimetry measurements [5,45].

If these defects are not the principal source of disorder in the acyl chains it is questionable if any principle disordering conformer is likely. A closer look at Fig. 6 reveals that the profile corresponding to the

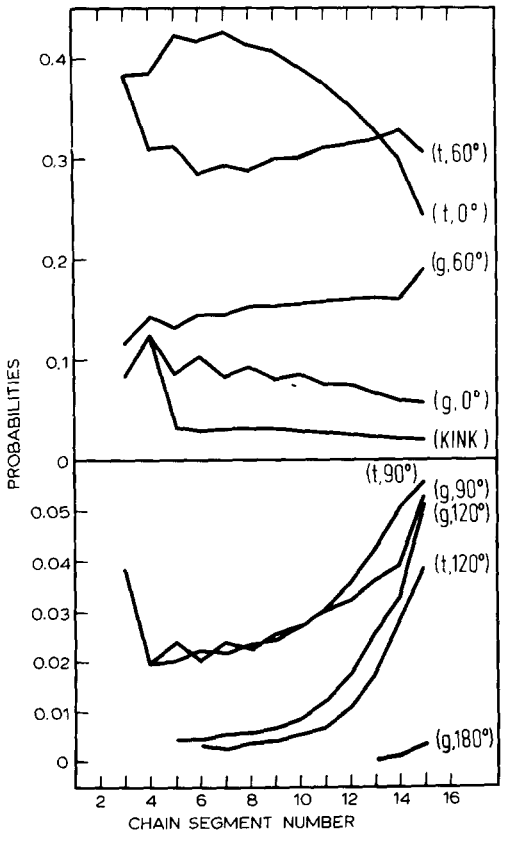

Fig. 6. Probabilities of a given segment configuration as a function of the segment number. The CH_2 segments are defined in Fig. 1B. The results are calculated for the acyl chain at $T = T_c$ and include the probability of the conformational defect labeled 'kink'. In the notation of Fig. 1B a 'kink' is defined by the segmental sequence ($g^{\pm}$, 60°), (t, 60°), ($g^{\mp}$, 0°). The segment configuration which have a angle, θ, larger than 90° correspond to the hairpin conformations. The influence of such conformations on the order profile have been shown in Fig. 5.

(t, 60°) configuration runs roughly parallel to the profile of the (g, 60°) configuration but with a probability which is twice as large. This is strongly indicative of a conformational trend since these two profiles are correlated. Indeed for geometrical reason a segment in a (t, 60°) configuration can only follow another (t, 60°) segment or a segment in the (g, 60°) configuration. Therefore the larger probability of the (t, 60°) configuration profile indicates a conformational trend where a segment in a (g, 60°) configuration is followed by several (t, 60°) segments in a row, as follows from the results given in Fig. 7. The figure contains besides the (g, 60°), (kink) and (jog) profiles, four profiles named (t, 60°; I) to (t, 60°; IV) which give the probability for each chain segment being in a (t, 60°) configuration as the first, second, third and fourth *trans* segment respectively immediately after a segment in a (g, 60°) configuration. The probabilities of such conformers following chain segment 2 have been eliminated from the figure since they reflect mainly the choice of the initial conditions. From the results shown in Fig. 7, it can also be seen how the (t, 60°) profile competes with the (kink) profile as does the (t, 60°; IV) profile with the (jog) profile. In both cases the tendency to maintain the (t, 60°) configuration over a (g, 0°) one is dominating. This tendency dominates also the other alternative, a (g, 90°) configuration. This conformational trend is certainly more compatible with the volume

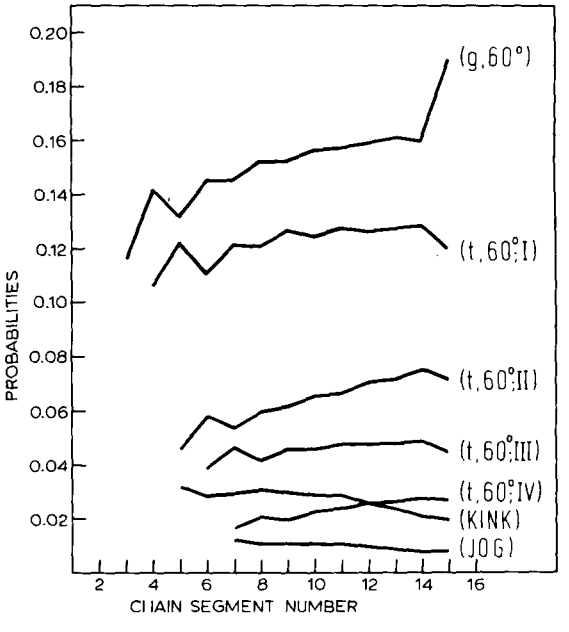

Fig. 7. Probabilities of a principal disordering conformers compared to the probabilities of 'kink' and 'jog'. In the notation of Figure 1B a jog is defined by the segmental sequence ($g^{\pm}$, 60°), (t, 60°), (t, 60°), (t, 60°), ($g^{\mp}$, 0°). The probabilities are calculated as a function of the segment number in the chain at $T = T_c$. The profiles noted as (t, 60°, I) to (t, 60°, IV) refer to the probability for a segment to be in a (t, 60°) state as the first, second, third or fourth segment respectively after a (g, 60°) segment.

change observed at the main transition [5], than is the kink picture.

In order to determine whether the configurational picture of the bilayer just obtained also holds above T_c, the average number of bonds $\langle N \rangle$ per chain in each one of the ten possible configurations as well as the average number per chain of kinks and jogs are plotted in Fig. 8 as a function of the temperature. Note that the changes seen in the lower part of the figure are amplified by the change in scale. The principal disordering conformer observed at T_c and discussed above is maintained and becomes even more likely in the range of temperature examined. Conversely, the probabilities of kinks and jogs are temperature independent.

In the gel phase at T_c 1.2 *gauche* bonds per chain are found, in agreement with Raman data [44]. The model indicates that half of them are involved in a kink conformation which has a probability of 0.3 per chain. In the gel phase the kinks account for 36% of the disorder and seem therefore to be more probable with close packing [46].

(d) Comparison with neutron scattering data and one dimensional spatial characteristics of the acyl chains

In the sections a and c the internal order or disorder of the acyl chains has been studied in terms of segmental angular fluctuations with respect to the axis of motional averaging or in terms of segmental configurational probabilities, these quantities being closely related. The spatial characteristics of the chain conformations also of interest provides complemetary information which is not unequivocally obtainable from the angular fluctuations. Neutron diffraction experiments on selectively deuterated hydrocarbon [7,47] chains can provide some of the necessary data to complement ^{2}H-NMR results. Neutron scattering results can be used to measure the projected mean conformation of the chains on the bilayer normal. The theoretical model can also be used to compute similar one-dimensional spatial charateristics of the acyl chains. Fig. 9 shows one form of this correlation in which the mean distances between the CH_2 groups as calculated from the model are compared with data from neutron scattering at $T = 323$ K. The measured distances from the center of the bilayer (neutron diffraction [6,7]) are plotted along the abscissa, whereas the computed distances are shown

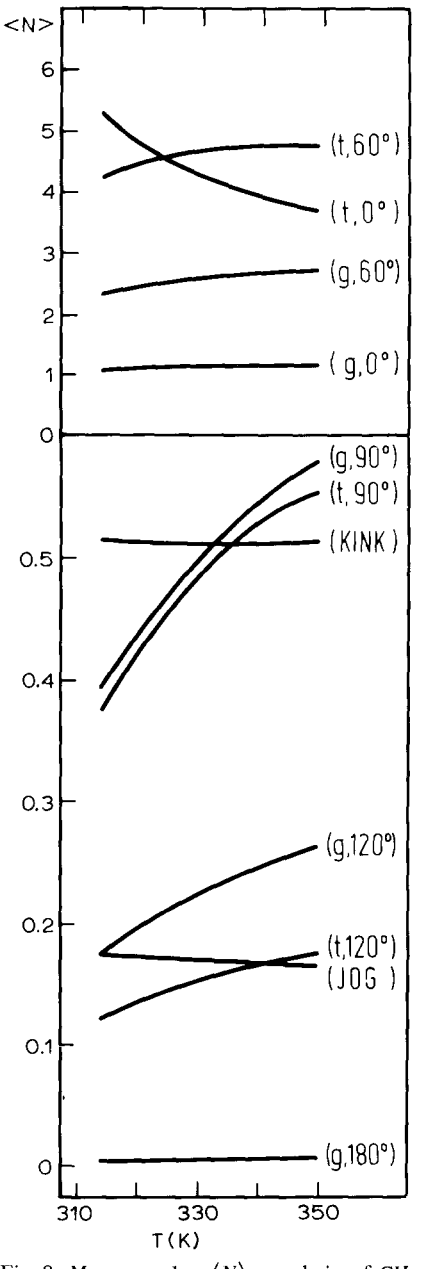

Fig. 8. Mean number $\langle N \rangle$ per chain of CH_2 segments in the different possible configurations and mean number $\langle N \rangle$ of 'kinks' and 'jogs' per chain. The values are calculated as a function of the temperature. Note that in the bottom part of the figure the scale has been magnified.

in the direction of the ordinate. The bars correspond to the experimental error. The points falling on the diagonal line correspond to a perfect agreement

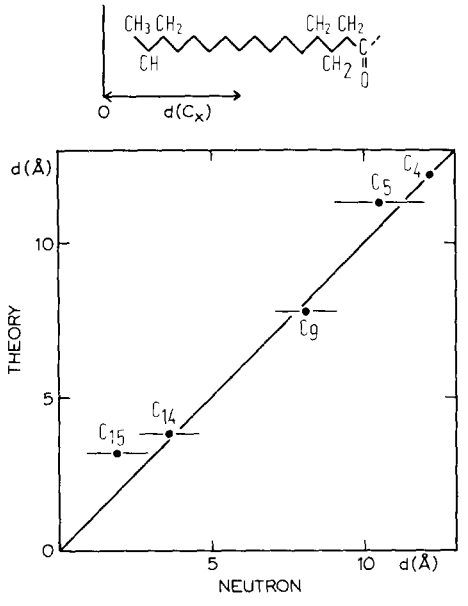

Fig. 9. Correlation of the mean distances between the CH_2 groups with neutron diffraction data. The mean distances are calculated from the theory and compared with data from neutron scattering. The experimental data, indicated by the points, are taken from Büldt et al. [6]. Since the centre of the bilayer is not defined in the theoretical calculation, it is necessary to adjust all the calculated distances by some constant amount. This was done by using the value for carbon C-4, which explains the absence of an error bar for this point.

between the experimental and theoretical data. Since the center of the bilayer is not defined in the theoretical calculation, it is necessary to adjust all the calculated distances by some constant amount. This was done by using the value for carbon C-4, which explains both its location on the diagonal and the absence of an error bar. With the exception of carbon atom C-15 the correlation is very good. It should be noted, however, that the neutron data yield a distance between C-14 and C-15 already larger than that of a *trans* segment [7].

Neutron scattering data also yields information about the extent of motion of the deuterated carbons along the long axis of the molecule, i.e. parallel to the bilayer normal. The shape of the distribution function of the labeled segment can be fitted by a Gaussian function. The standard deviation of the Gaussian becomes a characteristic of the positional fluctuations along the chain of the labeled carbon atom. This information has been obtained for carbon atoms C-4, C-9 and C-12, but under experimental conditions which differ somewhat from those assumed in the model [7] in three ways. (I) The theoretical computation does not include an overall fluctuation of the molecule along the bilayer normal. (II) The experimental positional fluctuations (neutron diffraction) were obtained on molecules having both chains deuterated and contain therefore a static distortion since one chain is shifted slightly with respect to the other. (III) for reasons of accuracy the neutron diffraction experiments have been done on a sample with a low water content (10% (w/w)). This modifies the physical state of the bilayer, since the phase transition temperature is increased to T_c = 328 K. Because of the effects noted in (I) and (II) a larger standard deviations can be expected for the experimental distributions. The best way to take into consideration point (II) is to carry out the comparison at the equal reduced temperature, [48] where $\theta = (T - T_c)/T_c$. The result is shown in Table III and indicates a satisfactory comparison between the theoretical and the diffraction results.

Because the theoretical model has been so successful in its simulation of both the order profile and the neutron diffraction results, it has been used to carry out an extensive study of the positional fluctuation of each CH_2 segment at T_c. The results are shown in Fig. 10. Carbon atom C-1, which is part of the carbonyl group, determines the origin of both scales. The length of an interval corresponds to the distance between two adjacent carbon atoms in the all-*trans* conformation. This scale has been purposely introduced to indicate that the distribution curves are actually the envelopes of histograms. The curve numbers correspond to the chain segment numbers. The ordinate gives the relative frequency, in percent, for a given segment to fall in a given interval or to be found at a given depth in the bilayer.

Contrary to the order profile, which shows a region of constant order, the positional fluctuation grows steadily toward the end of the chain. This is by no mean a contradiction, since the increase in the positional fluctuation reflects mainly the fact that the motion of a given segment depends upon the motion of the preceding segments. This is best illustrated by the following simple example. Assume a chain of n successive segments ($\bar{\nu}$ vectors in Fig. 1), which is

TABLE III

COMPARISON BETWEEN THE EXPERIMENTAL AND THEORETICAL STANDARD DEVIATIONS OF THE POSITIONAL DISTRIBUTION FUNCTIONS

Carbon atom	S.D. (Å)		T(K)	θ	θ
	Exp. [a]	Theor.	Exp.	Theor.	
C- 4	1.1 ±0.4	0.72	343	328	0.045
C- 9	1.81 ± 0.4	1.82			
C-12	2.4 ±0.4	2.26			

[a] Taken from Ref. 7.

found only in the two following conformational states, all the segments either in a 0° orientation or in a 60° orientation. If l_0 is the length of a segment, the last one has a range or positional fluctuation of $n \cdot l_0 \cdot (1 - \cos 60°)$ whereas the first one of only $l_0 \cdot (1 - \cos 60°)$. Both the first and last segments have nevertheless the same angular fluctuation. The standard deviations of the different distribution curves cannot therefore be used unequivocally to describe ordering along the chain. However, the degree of asymmetry of the distribution curves is a characteristic of order as it is directly related to the existence of the all-*trans* conformation. For example, the right end points of each of the curves give the probability of finding, at this segmental location, the chain is the all-*trans* conformation. In other words these end points defined a curve which shows how the probability of the all-*trans* conformation decays as one moves from the beginning toward the end of the chain. (The most rigid end point gives the probability of the all-*trans* conformation.)

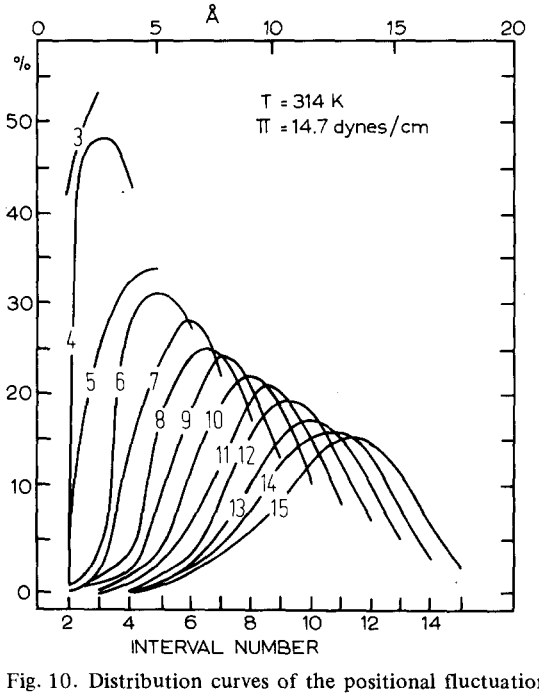

Fig. 10. Distribution curves of the positional fluctuations of each segment along the long axis of the acyl chains. The abscissa is expressed in either Angstroms or interval number and is described more fully in the text. The ordinate gives the relative frequency, in percent, for a given segment to be found in the indicated interval or to be found at a given depth in the bilayer.

The natural logarithm of these probabilities is linearly related to the chain segment number for the first eight segments. It corresponds to a simple exponential decay of the probability. Beyond this point, the relationship is no longer linear. There is an increasing deviation from linearity. The motion of the first eight CH_2 segments, unlike those in the rest of the chain, is therefore highly correlated. This fact is in agreement with the finding that they give a plateau in the order profile and that their rotational correlation times determined from the T_1 relaxation time data also exhibits a plateau when plotted as a function of the chain segment number [49]. Thus the theoretical model and all the experimental data give the same overall picture of order in the bilayer.

Because the curves of Fig. 10 have been obtained with the numerical values of Table I, these positional fluctuations are consistent with the order profile of Fig. 2A (top curve). It is still necessary to demonstrate that the distribution functions of Fig. 10 are consistent with a homogeneous density of CH_2 segments in the hydrophobic part of the bilayer. This is done by first including segment 16 in Fig. 10 and then summing the 15 distribution curves over the same number of intervals. The terminal CH_3 group is given a statistical weight of 2 because its volume is twice as great as that of a CH_2 group [11]. Next the resulting segment density profile is combined with another profile according to the overlap of two monolayers in a bilayer obtained by extrapolating the neutron scattering data to the phase transition temperature [7]. The resulted segment density profile throughout the width of the hydrophobic part of the

bilayer is shown in Fig. 11. A density of one corresponds to one CH_2 segment in an interval. The broken lines describe the segment density profiles of a hypothetical monolayers. For comparison the mean locations of several carbon atoms as well as the mean maximal length of a chain as computed from the model are reported on the top of Fig. 11. Considering that the segmental density profile has a standard deviation of 9% and taking into account the use of approximations in the histogram procedure it may be considered as roughly constant. The theoretical model is therefore consistent with the constant density requirement.

(e) Three-dimensional spatial characteristics of the acyl chains

The question of how chain isomerization is related to the spatial distribution of acyl chains is now addressed. Detailed structural information is beyond the scope of these studies. However, it will be seen subsequently that the results do illustrate the usefulness of a theoretical approach to complement experimental results. To understand the next section better it is necessary to outline how the computation of the spatial distribution is done.

In essence, the calculations involved in Fig. 10 are extended to three dimensions. But again the points represent a probability distribution function for each CH_2 segment. By taking a section perpendicular to the membrane plane through the three-dimensional probability distribution function, the one dimensional distributions shown in Fig. 10 are obtained. The distribution functions of the CH_2 segments are examined in planes perpendicular to the bilayer normal and located in the middle of the intervals described in Fig. 10. Such a calculation must be shown by probability contours, i.e., two dimensional curves or maps.

Representative results of these computations are depicted by the isoprobability maps shown in Fig. 12 for CH_2 segment 8 in the planes 8, 6, 4 and 2 and for CH_2 segment 5 in the planes 5 and 3. The plane defined by the successive C-C bonds in the all-*trans* conformation corresponds to the plane of symmetry apparent in the maps. The symmetry arises from the equivalence of the configurations (g^+, 60°) and (g^-,

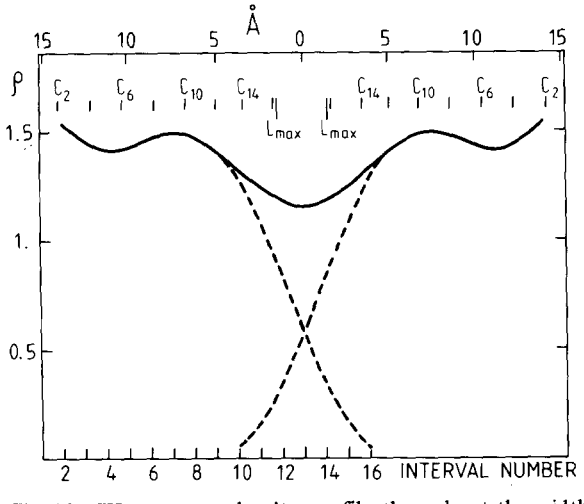

Fig. 11. CH_2 segment density profile throughout the width of the bilayer. The boken lines correspond to a monolayer and indicate the extent of overlap of the two monolayers within a bilayer. For comparison, the top of the figure contains the mean location of several carbon atoms as well as the maximal length indicated at the point labelled L_{max}.

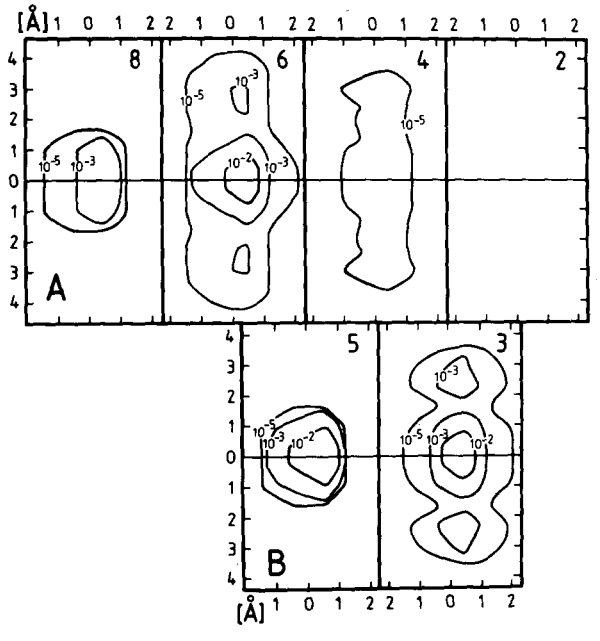

Fig. 12. Probability contours of chain segment locations. (A) This probability map contains the CH_2 segment 8 in the planes 8, 6, 4 and 2, while (B) contains segment 5 in the planes 5 and 3. Each contour line corresponds to one of the five following probability values: 10^{-5}, 10^{-3}, 10^{-2} and $3 \cdot 10^{-1}$. If a contour is missing it means that it does not have a finite value. The coordinate system of each map is explained in Fig. 1C.

60°) occurring after a segment in the (t, 0°) configuration. This symmetry is verified experimentally by ^{2}H-NMR by the fact that the two deuterons of a methylene group yield the same quadrupole splitting [3]. The contours are not cylindircally symmetric, since they are recorded in a frame of reference rotating with the phospholipid molecule. Whereas segments 5 and 8 show a difference in their positional fluctuations (see Fig. 10), their lateral fluctuations visible in the contour maps, seem to be relatively similar. In Fig. 13 the isoprobability values of segment 15 in the planes 15, 13, 11, 9, 7, 5 and 3 are plotted. It can be noted that with respect to segment 5 and 8 the positional fluctuation has increased faster than the lateral one.

In order to study the overall motion of a chain accompagnying isomerization, the probability distribution functions of the individual segments are summed. The result is a density distribution function for the chain as a whole. The cross-sections of this function on the planes 2 to 15 are shown in Fig. 14. To save space, the forementioned symmetrical portions are omitted. The overlap of two such figures (not shown here), in analogy to Fig. 11, exhibits similar density distribution over the whole width of the hydriphobic part of the bilayer indicating a homogenous volume occupancy of the chain.

The elongated shapes displayed by the probability distribution contours in the different planes pose a problem about the accomodation of two chains within the frame of a molecule. According to X-ray data the two chain long axis cannot be separated by more than approx. 5 Å [50]. Therefore the internal motion of one acyl chain is going to influence that of the other chain, the amount depending upon their relative orientation. A maximum of cooperativity

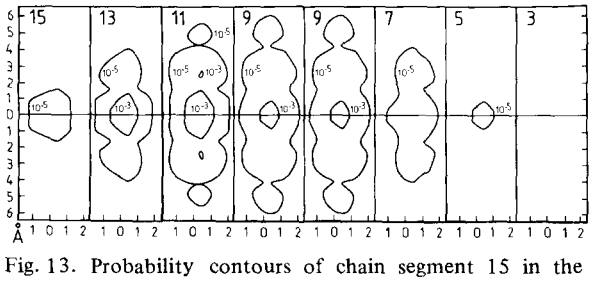

Fig. 13. Probability contours of chain segment 15 in the planes 15, 13, 11, 9, 7, 5 and 3. See also Fig. 12 for the definition of the coordinate system and contouring scheme.

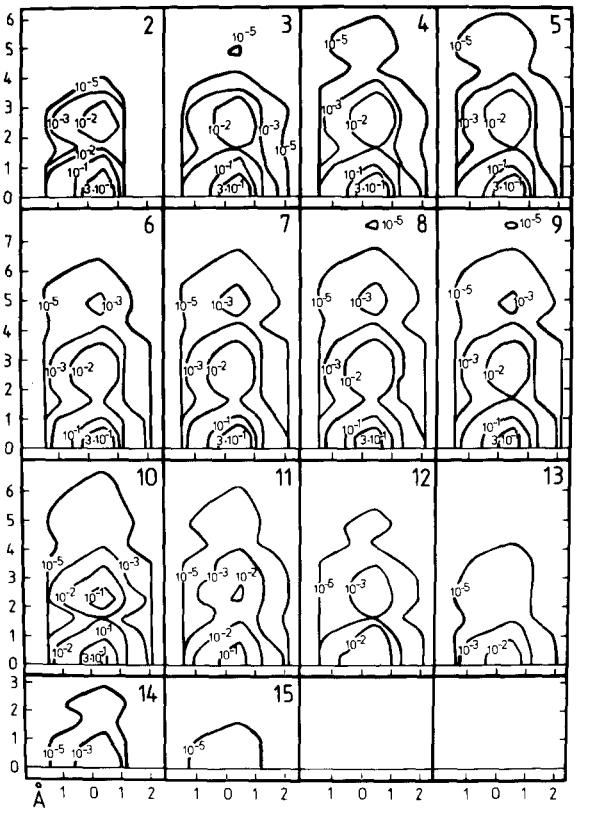

Fig. 14 Density contours of the whole acyl chain in the half planes 15 to 2. This figure differs from Figs. 12 and 13 in that here the probability and location of any CH_2 segment are recorded. Several segments may be found at the same depth in the bilayer.

between both chains is expected when the planes defined by the C-C bonds in the all-*trans* conformation are perpendicular to the plane defined by the long axis of the two acyl chains whereas a parallel orientation implies a minimum of cooperativity. ^{2}H-NMR measurements of DPPC-chloresterol-water systems have shown the possibility of producing order in chain 2 while chain 1 still retains some internal motion [51]. Bond on these results it seems that both acyl chains behave more or less independently, favouring a picture of relatively low cooperativity. With such arrangement the phospholipid molecule looks on the average more of less like a cylinder, which may amplify the overall rotation of the molecule. Moreover such an overall shape is more in line with the measured area per molecule [48,52]. Finally

such a low cooperativity justifies a posteriori the approximation in the model of considering independent chains within a molecule.

Conclusions

The numerical values obtaind from fitting NMR data to the theoretical model gives good agreement with very different kinds of experimental data such as neutron diffraction, etc. It is suggested that the theoretical model can be used as a reliable tool to provide information about experimentally inaccessible questions. Moreover, the high accuracy exhibited by the theory provided an opportunity to understand in detail the shape of the experimental profile. In particular it was possible to associate the length of the plateau of the order profile with the amount of chain isomerization. This finding opens new possibilities regarding the use of the order profile to detect physical changes in the bilayer. Indeed, it is suggested here that the length of the plateau region should be given more attention in the interpretation of ^{2}H-NMR data. It could be used as a direct probe of the state of the acyl chains or as an indirect probe of possible interactions in the region of the head groups. This analysis of the experimental order profile is a typical result which can be reached only by considering explicitly all the conformations and is therefore beyond the scope of a simplified model not requiring undefined physical parameters [45]. The model can be used in a number of other ways as a numerical tool. For example, the low probabilities of defects like kink and jog could not only be confirmed but also explained by comparing them with the probabilities of other principal disordering conformers more in line with the dilatometry results.

Although the model calls for several approximations, the formalism realistically considers the true nature of the interactions between the lipid molecules. One of the goals of this study was therefore also to test the practicability of the model with respect to the physical concepts underlying the theory. This has been achieved in Fig. 2 and 3 where the Marcelja model [8] and the present model have been compared in their respective abilities to reproduce the ^{2}H-NMR data.

Because the theory appears to give reliable results it has also been applied to the description of the spatial characteristics of the acyl chains, an area still largely inaccessible to experimental techniques. Firstly it was shown that a knowledge of the S_{C^2H} order parameters does not allow one define how the chain CH_2 segments are distributed in space because a single angular fluctuation might correspond to a number of possible spatial fluctuations. An indication of order along the chain is the probability of the all-*trans* conformation which decreases exponentially from the origin within the plateau region, but in a more complex manner beyond this region. The longitudinal fluctuations grow faster going toward the end of the chain than the lateral ones. Finally, the order profile reproduced on the basis of chain isomerization is consistent with space homogeneously filled, on average, by the CH_2 chain segments. In the model the specific interactions between head groups and between head group and water have been reduced to a lateral area energy term, πA. Despite this unspecific treatment, the role of the head groups in the organiation of the bilayer is emphasized by considering the effect of varying the lateral pressure π on the order of the acyl chains. In other words, it has been implicity demonstrated that the anisotropic nature of the interactions between the acyl chains is a direct consequence of the interactions in the polar head group region.

Although the theoretical model has been able to reach the goals for which it has been devised, this achievement cannot be used to justify a posteriori the approximations involved in the theory. The usefulness and meaning of the theoretical model lies mostly in its ability to describe accurately the state of a bilayer. The exact physical basis for explaining all of the properties of a lipid bilayer are left to more rigorous models [45]. It would appear from the results presented here that the semi-empirical and rigorous approaches are complementary.

Acknowledgement

We are sincerely indebted to Prof. J. Seelig for many valuable and fruitful discussions during this study. This work was supported by the Swiss National Science Foundation grant No. 3.390.74. One of us (J.S.) wishes to thank the European Molecular Biology Organisation for a travel grant.

References

1 Seelig, J. and Seelig, A. (1980) Q. Rev. Biophys. 13, 19–61
2 Meraldi, J.-P. and Schlitter, J. (1981) Biochim. Biophys. Acta 645, 183–192
3 Seelig, J. (1977) Q. Rev. Biophys. 10, 353–418
4 Flory, P.J. (1969) Statistical Mechanics of Chain Molecules, Interscience, New York
5 Nagle, J.F. and Wilkinson, D.A. (1978) Biophys. J. 29, 159–175
6 Büldt, G., Gally, H.U., Seelig, A., Seelig, J. and Zaccai, G. (1978) Nature 271, 182–184
7 Zaccai, G., Büldt, G., Seelig, A and Seelig, J. (1979) J. Mol. Biol. 134, 693–706
8 Marčelja, S. (1974) Biochim. Biophys. Acta 367, 165–176
9 Petersen, N.O. and Chan, S.I. (1977) Biochemistry 16, 2657–2667
10 Schindler, H. and Seelig, J. (1975) Biochemistry 14, 2283–2287
11 Tardieu, A., Luzzati, V. and Reman, F.C. (1973) J. Mol. Biol 75, 711–713
12 Charvolin, J., Manneville, P. and Deloche, B. (1973) Chem. Phys. Lett. 23, 345–347
13 Seelig, J. and Niederberger, W. (1974) Biochemistry 13, 1585–1586
14 Seelig, A. and Seelig, J. (1974) Biochemistry 13, 4839–4845
15 Seelig, J. (1980) in Biophysics of Membranes and Intercellular Communications (Les Houches, Session XXXIII) (Balian, R., Chabre, M. and Devaux, P., eds.), North-Holland Publishing Company, Amsterdam
16 Doniach, S. (1978) J. Chem. Phys. 68, 4912–4916
17 Billmeyer, F.W., Jr. (1957) J. Appl. Phys. 28, 1114–1118
18 Hui, S.W.M., Cowden, D., Papahadjopoulos, D. and Parsons, D.F. (1975) Biochim. Biophys. Acta 382, 265–274
19 Nagle, J.F. (1976) J. Membrane Biol. 27, 233–250
20 Albrecht, O., Guler, J. and Sackmann, E. (1978) J. Phys. 39, 301–313
21 Blume, A. (1979) Biochim. Biophys. Acta 557, 32–44
22 Stanley, H.E. (1971) Introduction to Phase Transitions and Critical Phenomena, Clarendon Press, Oxford
23 Nagle, J.F. and Scott, H.L., Jr. (1978) Biochim. Biophys. Acta 513, 236–243
24 Owicki, J.C., Springgate, M.W. and McConnell, H.M. (1978) Proc. Natl. Acad. Sci. USA 75, 1616–1619
25 Mely, B., Charvolin, J. and Keller, P. (1975) Chem. Phys. Lipids 15, 161–173
26 Turner, G., and Oldfield, E. (1979) Nature 277, 669–670
27 Smith, I.C.P., Tulloch, A.P., Stockton, G., Schreider, S., Joyce, A., Butler, K.W., Boulanger, A., Blackwell, B. and Benett, L.G. (1978) Ann. N.Y. Acad. Sci. 308, 8–28
28 Scott, H.L., Jr. (1975) J. Chem. Phys. 62, 1347–1353
29 Jacobs, R.F., Hudson, B. and Andersen, H.C. (1975) Proc. Natl. Acad. Sci. USA 72, 3993–3997
30 Jackson, M. (1976) Biochemistry 15, 2555–2561
31 Kox, A.J. and Wiegel, F.W. (1978) Physica 92A, 466–474
32 Dill, K.A. and Flory, P.J., (1980) Proc. Natl. Acad. Sci. USA 77, 3115–3119
33 De Gennes, P.G. (1974) Phys. Lett. 47A, 123–124
34 Priest, G.R. (1977) J. Chem. Phys. 66, 722–725
35 Seelig, A. and Seelig, J. (1975) Biochim. Biophys. Acta 406, 1–5
36 Seelig, J. (1978) Prog. Colloid Polymer Sci. 65, 172–179
37 Saupe, A. (1964) Z. Naturforsch. 19a, 161–171
38 Perschold, W. (1968) Koloid, Z.Z. Polymer 228, 1–38
39 Träuble, H. (1971) J. Membrane Biol. 4, 193–208
40 Scott, H.L., Jr. and Cheng, W.H. (1979) Biophys. J. 28, 117–132
41 Rice, D.M., Meadow, D.M., Scheinman, A.O., Goni, M.F., Gomez-Fernandez, J.C., Mocarello, M.A., Chapman, D., and Oldfield, E. (1979) Biochemistry 18, 5893–5903
42 Nagle, J.F. (1973) J. Chem. Phys. 58, 252–264
43 Nagle, J.F. (1973) Proc. Natl. Acad. Sci. USA 70, 3443–3444
44 Yellin, N. and Levin, I.W. (1977) Biochemistry 16, 233–250
45 Nagle, J.F. (1980) Annu. Rev. Phys. Chem. 31, 157–195
46 Scott, H.L., Jr. (1977) Biochim. Biophys. Acta 469, 264–271
47 Büldt, G., Gally, H.U., Seelig, J. and Zaccai, G. (1979) J. Mol. Biol. 134, 673–691
48 Seelig, J. and Browning, J.L. (1978) FEBS Lett. 92, 41–43
49 Brown, F.M., Seelig, J. and Häberlen, U. (1979) J. Chem. Phys. 70, 5045–5053
50 Hitchcock, P.B., Mason, R., Thomas, K.M. and Shipley, G.G. (1974) Proc. Natl. Acad. Sci. USA 71, 3036–3040
51 Haberkorn, R.A., Griffin, R.G., Meadows, M. and Oldfield, E. (1977) J. Am. Chem. Soc. 99, 7353–7355
52 Chapman, D., Williams, R.M. and Ladbrooke, B.D. (1967) Chem. Phys. Lipids 1, 445–475